AADE-15-NTCE-28

Integration of XFEM and CZM to Model 3D Multiple-Stage Hydraulic Fracturing in Quasi-brittle Shale Formations: Solution-Dependent Propagation Direction

Mahdi Haddad and Kamy Sepehrnoori, The University of Texas at Austin

Abstract

The Cohesive Zone Model (CZM) honors the fracture tip effects in a quasi-brittle rock such as shale, which results in a more precise fracture geometry and pumping pressure compared to those from Linear Elastic Fracture Mechanics. Nevertheless, this model, namely planar CZM, assumes a predefined surface on which the fractures propagate and therefore, restricts the fracture propagation direction. Notably, this direction can be acquired integrating CZM as the segmental contact interaction model with a fully coupled pore pressure-displacement, extended finite element model (XFEM).

In this work, we modeled triple-stage 3D hydraulic fracturing in a single-layer, quasi-brittle shale formation using planar CZM and XFEM-based CZM including slit flow and poro-elasticity for fracture and matrix spaces, respectively, in Abaqus. Our fully-coupled pore pressure-stress Geo-mechanics model includes leak-off as a continuum-based fluid flow component coupled with the other unknowns in the problem.

Having compared the triple-stage fracturing results from planar CZM with those from XFEM-based CZM, we found that the stress shadowing effect of hydraulic fractures on each other can cause these fractures to rationally propagate out of plane. We investigated the effect of this arbitrary propagation direction on not only the fractures' length, aperture, and the required injection pressure, but also fractures' connection to the wellbore. Depending on the spacing, this connection can be disrupted due to the near-wellbore fracture closure which may embed proppant grains on the fracture wall, or screen out the fracture at early times.

Introduction

Shale gas resources have profoundly contributed to the prospective independence of the U.S. on oil and gas from foreign resources. The abundant condensate gas production and export from the U.S. shale resources have significantly contributed in the global sharp oil price decline since August 2014.[1] These resources are constituted of ultra-low permeable, organic-rich formations with desorption of gas as a major but slow-rate and long-lasting producing mechanism. Economic production from these resources through gas desorption requires a complex network of natural fractures connected to the producing horizontal wellbores by hydraulic fractures in multiple stages, the most common stimulation technology in shale gas reservoirs. The geometry of hydraulic fractures (length, height, aperture, and propagation pattern) significantly contributes to long-term gas production and is inspected roughly by post-fracturing data acquisition methods such as tiltmeter fracturing mapping and micro-seismic monitoring.[2] This later method, however, cannot identify opening-mode or hydraulic fractures since the only detectable events using this method are shear slippage events. The technical restrictions on the hydraulic fracture data acquisition, the limitation on the extendibility of a successful fracturing job data to the other fields[3], and the high cost of re-stimulation plans, if possible, urge to develop numerical tools for optimal hydraulic fracturing design. Furthermore, due to the occurrence of cap rock and shale gas reservoir in close proximity and the environmental concerns about ground water contamination by fracking jobs, the induced fractures need to be cautiously placed in order not to propagate into the upper and lower geological layers. Such a rigorous hydraulic fracture design in shale rocks demands numerical optimizing tools which should also be versatile for a variety of shale formations in mineralogy and stress state and capture increasingly more complex fracture networks than expected in these resources.[2,4]

Hydraulic fracturing is defined as a fully coupled porous solid-fluid interaction problem where the fracturing force, the fluid pressure on the fracture walls, exceeds the minimum in situ principal stress plus the tensile strength of the rock.[5] The coupled phenomena include the fracturing fluid flow within the fracture, the fluid flow in the surrounding porous media, the permeation (leak-off) of the fracturing fluid into the formation, the matrix mechanical deformation, and the fracture growth.[6] Fluid leak-off and spurt loss depend on the fracturing fluid pressure, more fluid bleed-off leads to more pressure drop along fracture and less fracture propagation, and rock deformation alters the matrix porosity and permeability and therefore the fluid flow in the surrounding porous media. The hydraulic fractures potentially open and close (hysteresis effect) due to fracturing pressure alteration[7] which can be a consequence of

step-wise or unstable fracture propagation.[8,9] Furthermore, the more complexity in the hydraulic fracture patterns is partially attributed to stress shadows of pre-existing or simultaneously growing fractures[9,10], or the residual stresses from the previous completion operations[11]. These physical complexities challenge the majority of the existing models which are based on Linear Elastic Fracture Mechanics (LEFM), and restricted to linear rock failure and single-stage planar fracture propagation such as planar 3D (PL3D) models based on boundary integral method[12].

The simulation of hydraulic fracturing has been conducted by a variety of numerical methods such as Boundary Element Method (BEM) also called displacement discontinuity method or boundary integral method[13,14], and Finite Element Method (FEM)[15]. BEM cannot rigorously take into account the material heterogeneities and requires re-meshing during fracture propagation[16] whereas the classical FEM restricts the fracture path to the element edges[15,17] or along a pre-defined path named cohesive layer[10]. Nonetheless, the adoption of Cohesive Zone Model (CZM) in FEM enables to include the material softening effects at the fracture tip process zone, which simulates the quasi-brittle fracture propagation in shale rocks compared to ductile and brittle fracture propagation in steel and glass, respectively[18]. Furthermore, despite the common perception about the restriction of CZM in modeling non-intersecting fractures, Gonzalez and Dahi[19] investigated intersecting hydraulic and natural fractures simply by modifying the cohesive elements' middle nodes at the intersection.

In contrast to the classical FEM, the eXtended Finite Element Method (XFEM) can simulate the fracture propagation along arbitrary paths independent of the mesh. Lately, this method has been extended in Abaqus for the simulation of hydraulic fracturing by adding "edge" phantom nodes with pore pressure degree of freedom besides the previously developed "corner" phantom nodes[20,21]; we call this method as XFEM-based CZM. Compared to the most commercial hydraulic fracturing simulators in the upstream oil and gas industry[12] or even the recently developed models[22], the new capability provides the following improvements: 1) more plausible model for quasi-brittle rocks; 2) fully coupled pore pressure/stress analysis for the matrix and arbitrarily propagating fracture; 3) leak-off model based on fluid continuity and coupled with matrix deformation; 4) ability to include reservoir heterogeneities; and 5) fracturing simulation under the disturbed stress state due to the previous completion steps.

The theme of the current work is to apply the recently developed XFEM-based CZM in Abaqus for the simulation of simultaneous triple-stage hydraulic fracturing at various spacing and compare the results with those from the conventional CZM with pre-defined planar cohesive layers. We narrow our investigation down to the simultaneous fracturing scenarios after the work done by Haddad and Sepehrnoori[10] who demonstrated the superiority of the simultaneous fracturing scenario to achieve the best fracture geometries. This work includes additional geometric and physical characteristics such as non-planar fracture propagation, stress interactions between hydraulic fractures, and onset of the coalescence or divergence of fractures.

Method

In order to avoid re-meshing during the hydraulic fracturing simulation, and to improve the fracture tip solutions, a mesh independent crack growth model, XFEM, was proposed in the works done by Belytschko and Black[23] and Moes et al.[24]. Compared to the other FEM-based crack simulation methods, XFEM demonstrates several advantages such as the following: 1) arbitrary fracture growth direction predicted based on the current stress state close to the fracture tip; 2) easier initial crack definition; 3) simpler mesh refinement studies; 4) improved convergence rates in the case of stationary cracks; and 4) application in general static and implicit dynamic procedures[20]. XFEM incorporates the discontinuous geometry, the fracture, and the discontinuous field by enriching the finite element basis functions, Eq. (1), after Belytschko and Black[23] based on the partition of unity method of Babuska and Melenk[25]. The enrichment functions must be selected based on the class of problems, which includes a priori knowledge of partial differential equation behavior into finite element space (singularities and discontinuities). The enrichment functions for the fracture modeling problems are Heaviside and crack tip asymptotic functions which represent displacement jump across crack face and crack tip singularity, respectively, **Figure 1**. The later enrichment is derived from the solution of bi-harmonic equation very close to the tip of a single semi-infinite crack.

$$u^h(x) = \sum_{I \epsilon N} N_I(x) \left[u_I + H(x) a_I + \sum_{\alpha=1}^{4} F_\alpha(x) b_I^\alpha \right], \quad (1)$$

where $u^h(x)$ is the displacement at location x, $N_I(x)$ is the conventional shape function, u_I is the nodal degree of freedom for the conventional shape function, $H(x)$ is the Heaviside enrichment function, a_I is the nodal enrichment degree of freedom for jump discontinuity on fracture walls, $F_\alpha(x)$ is the crack tip enrichment (asymptotic) function, Eq. (2), and b_I^α is the nodal degree of freedom for the crack tip enrichments.

$$\{F_\alpha(r,\theta)\}_{\alpha=1,2,3,4} = \left\{ \sqrt{r}\sin\frac{\theta}{2}, \sqrt{r}\cos\frac{\theta}{2}, \sqrt{r}\sin\frac{\theta}{2}\sin\theta, \sqrt{r}\cos\frac{\theta}{2}\sin\theta \right\}, \quad (2)$$

where (r,θ) represents the location of the nodes of the element containing the crack tip in a local polar coordinate system centered on the crack tip.

The Heaviside enrichment uses the Phantom node approach to model splitting of an element into two parts[26] based on the superposed element formulation[27]. Furthermore, CZM is applicable in XFEM to quantify the magnitude of the discontinuity, the displacement jump across the crack faces, and to establish crack initiation and propagation criteria using mixed-mode formulae such as BK law. **Figure 2** demonstrates the cohesive traction-separation response indicating the damage initiation and evolution and the required parameters for a generalized CZM model. Moreover, as shown in **Figure 3**, the incorporation of planar CZM in a fully coupled pore pressure-stress analysis concludes a complicated pore fluid flow pattern in the porous media close to the fracture walls and tip, which

disapproves the application of Carter's linear, 1D leak-off model[28].

Nevertheless, the cohesive response in XFEM-based CZM does not include the elastic part in Figure 2 and the cohesive layer undergoes progressive damage at zero separation when the fracture initiation criterion is satisfied, **Figure 4**. Notably, the elastic response is inherently included in the elastic deformation of the porous media ahead of the fracture tip before further fracture propagation.

Furthermore, in XFEM, a method is required to locate the discontinuity; for instance, level set method (LSM). A level set of a real-valued function is the set of all points at which the function attains a specified value. This method is a popular technique for representing surfaces in interface tracking problems since for instance, XFEM cracks require the value of this function only at nodes belonging to elements cut by the crack. Generally, two functions Φ and Ψ are used for a complete description of crack faces and tips. However, only one level set function, Φ is sufficient to locate a crack if the crack propagates always up to the element edges. Using LSM in XFEM eases the calculation of contour integrals compared to traditional mesh-dependent methods since the level set functions' values at the nodes in an element automatically provide the required data for the contour integral.

XFEM must be cautiously applied for the simulation of fracturing in Abaqus due to the following[29]: 1) it requires very fine mesh close to the fracture propagation region to predict the correct growth direction; 2) the enrichment zone should exclude the "hotspots" such as boundaries or the other modeling artifacts in order to avoid unrealistic fracture propagations; 3) the phantom nodes on the boundaries must be constrained; and 4) the initial fractures (perforations) should cross fewer elements for the fast convergence of the solution at early times.

Model Construction

Hydraulic fracturing simulation using XFEM-based CZM is computationally more expensive than that using planar CZM as the reasonable convergence of the solution during fracture deviation in XFEM requires a very fine mesh in a large enrichment zone whereas the pre-defined fracture path in planar CZM needs refined mesh very close to the cohesive layer(s). Due to the restrictions in dynamic mesh refinement during XFEM analysis in Abaqus and the computational limits on the number of elements, we modeled hydraulic fracturing in a 3D geometry using a single layer of adequately fine mesh using 3D solid elements with pore pressure degree of freedom, C3D8P. Thus, the current work limits height growth to a single layer of elements; notably, our implemented XFEM-based CZM method is capable of simulating fully 3D hydraulic fracturing with higher computational expenses. Moreover, the solution from this model configuration can be simply verified comparing that with the analytical solution by Geertsma and de Klerk[30]. Due to the advantages of simultaneous hydraulic fracturing compared to sequential one[10], we restricted our investigation to a simultaneous fracturing scenario with three fractures (clusters) per stage, **Figure 5**. We defined one enrichment zone per fracture with the variable enrichment zone size; the middle fracture supposedly propagates straight, which requires a thin enrichment zone, Enrichment Zone 2. For better mesh size transition, we used the sweep meshing technique with advancing front[20]. The input parameters of the model can be found in **Tables 1** and **2**. We discretely perturbed some default values in order to investigate the effect of various parameters in our fully coupled poro-elastic solution, and also approach the real field data.

Results and Discussion

Figures 6 through **8** demonstrate the fracture propagation results for 7-, 13-, and 20-meter spacing, respectively. According to these figures, fracture spacing can influence fracture propagation in a variety of patterns from fracture coalescence to divergence. At 7-meter spacing (Figure 6), the side fractures propagate slightly toward the left and right boundaries at early times while they coalesce the middle fracture after 1683 seconds of simulation. In this solution, fracture propagation is restricted to an exclusive enrichment zone, which hurdles the physical coalescence of multiple fractures; however, the implemented model predicts the eminent proximity of fracture coalescence provided that the thickness of the enrichment zones is selected cautiously. The right contours in Figures 6 through 8 show the maximum principal stress to better demonstrate the stress shadowing effect of fractures on each other, which better explains the fracture propagation pattern.

Furthermore, the propagation of the side fractures in 7-meter (Figure 6) and 13-meter (Figure 7) spacing closes the middle fracture at the injection point, which may crush the proppant grains, embed them on the fracture walls, or transport them with the bulk of the fracturing fluid toward the fracture tip; all these effects adversely influence the gas productivity of the middle fracture. The same phenomenon can be observed in the case with 20-meter spacing, Figure 8, where the side fractures close up at the injection points due to the growth of the middle fracture. Moreover, the further propagation of the side fractures in 20-meter spacing causes a compressional region right ahead of the middle fracture (the circular, small blue region ahead of the middle fracture tip in the right picture of Figure 8), which prevents the middle fracture to grow as long as the other fractures.

Moreover, the fractures in 13-meter spacing remain almost parallel up to the end of the simulation whereas the middle fracture grows longer than the others. This special configuration causes the proximity of a high fluid pressure zone, within the middle fracture, and the low pore pressure zones around the left and right fracture tips, which concludes the fluid communication between the side fractures and the middle fracture. This fluid communication can be correlated to the tensile maximum principal stress zones between the side fracture tips and the middle fracture considering more severe fluid leak-off from the middle fracture toward the side fractures, Figure 7. As stated before, our fully coupled pore pressure-stress analysis using XFEM-based CZM can provide rigorous solutions for the complex physics around the fracture tips including the nonlinear fluid flow patterns around fractures.

Figure 9 compares the injection pressure and fracture aperture at the injection point for the middle perforation. The results for 20-meter spacing follow different trends from those for the other spacing values; this is consistent with the middle fracture configuration, Figure 8, as the middle fracture at 20-meter spacing grows shorter in length and therefore, expands more in aperture, which leads to a wider aperture at the injection point. As stated before, the compressional region ahead of the middle fracture resists further propagation of the middle fracture, which significantly contributes in the high injection pressure and fracture aperture at the injection point for the middle fracture.

Comparison of XFEM-based CZM and Planar CZM

Our triple-stage hydraulic fracturing problem can be solved also using planar CZM with the cohesive layers on three pre-defined planes. All mechanical properties are the same as before expect the following: 1) fracture initiation criterion, which must be switched to quadratic nominal stress, QUADS, as the maximum principal stress criterion, MAXPS, does not lead to any fracture propagation on the cohesive layers; 2) cohesive layer stiffness, which is 65 times that of the adjoining material in planar CZM, and un-defined in XFEM-based CZM, Figure 4.

Figures 10 and **11** respectively demonstrate the injection pressure and fracture aperture at the injection point for various stages using planar and XFEM-based CZM models. Both models conclude the same general trend for the studied parameters whereas the XFEM-based CZM predicts higher values for these parameters compared to those from the planar CZM.

As shown in Abaqus Benchmarks Guide[31] for the propagation of hydraulically driven fracture using XFEM, the solution from XFEM-based CZM is highly sensitive to mesh refinement such that an extremely fine mesh can conclude an XFEM solution very close to the planar CZM solution. Nonetheless, the investigated problem in the above reference is a single-stage 2D hydraulic fracturing problem with a known propagation path which restricts mesh refinement to a narrow region around itself. However, in a multi-stage hydraulic fracturing problem, the mesh refinement region cannot be restricted to a small area as fractures can propagate on arbitrary paths due to the stress shadowing effect and mesh refinement in a big region is required, Figure 8. Therefore, even with a very fine mesh, we could not prove mesh independency of the solution for injection pressure, Figure 10.

Furthermore, the planar CZM results in a lower fracture aperture at the injection point compared to that from the XFEM-based CZM, Figure 11. This trend can be attributed to the following issues: 1) inadequate mesh refinement around the fractures; and 2) the restriction of the fractures to propagate on pre-defined paths in the planar CZM in contrast to the freedom of the fractures to propagate on arbitrary paths in the XFEM-based CZM.

Parametric Study

The above results were drawn at low horizontal stresses and low stress contrast (the difference between minimum and maximum horizontal stresses), which concluded long fracture propagation and high deviations. In order to demonstrate the effect of the stress contrast and absolute values of the stresses on fracture deviation, we investigated fracture propagation at 7-meter spacing for a range of maximum horizontal stresses, keeping the minimum horizontal stress constant, and amplifying pore pressure and stresses 10 times those in the previous results or Table 1. This stress amplification shifts input data toward more realistic field values. As observed in **Figure 12**, higher absolute values for stresses and pore pressure conclude lower fracture deviation meaning that the fractures intend to grow longer without coalescence or divergence. Moreover, increasing the stress contrast or the maximum horizontal stress leads to less deviation of the side fractures and the middle fracture closure, which agrees with the middle fracture configuration at low stresses, Figure 6. Therefore, fracture propagation and deviation highly depends on the maximum horizontal stress or stress contrast, and the absolute values of the stresses.

In order to quantify the effect of the stress contrast on the properties of hydraulic fractures, we compared the injection pressure and fracture aperture at the injection point for left, middle, and right perforations in **Figures 13**, **14**, and **15**, respectively. These figures show that the maximum horizontal stress negligible effects the injection pressure and fracture aperture at the injection point for various perforations. Nevertheless, a variation in the injection pressure can be observed for different maximum horizontal stresses around 150 seconds of injection, which can originate from the nonplanar fracture propagation and the stress interaction of fractures with each other.

Figures 13 and 15 demonstrate consistent left and right fracture closure at the injection point as the opening of the left fracture coincides with the closure of the right fracture after 1000 seconds of injection. Moreover, Figure 14 shows that the middle fracture closes up to 2 millimeters, the fracture aperture at early times, after 300 seconds of injection, which demonstrates the negligible contribution of the middle fracture in production.

Conclusions

Using a fully coupled pore pressure-stress, quasi-static, finite strain analysis, we solved 3D triple-stage hydraulic fracturing problems. The fractures were modeled using CZM and XFEM-based CZM; the first model is advantageous with respect to LEFM for quasibrittle rocks such as shales due to a more rigorous treatment with the process zones ahead of the fracture tips. In addition to this advantage, the second model releases the restriction on the fracture propagation plan in CZM. Mechanical interactions or stress shadowing effects of closely spaced hydraulic fractures concluded the following remarks:

(1) XFEM-based CZM can simulate hydraulic fracturing on an arbitrary solution-dependent path in contrast to CZM which restricts fracture growth on a pre-defined plane.

(2) Coalescence and outward deviation of side fractures at various spacing.

(3) Possible fracture closure at the injection point for all clusters depending on the spacing.

(4)The extra opening of one side fracture can lead to the extra closure of the other side fracture.

Building a model and grid dependence analysis using XFEM-based CZM are easier than CZM due to the element type, initialization and element crossing

XFEM-based CZM requires adequately fine mesh close to fractures, however, the temporal fracture propagation direction depends on an increasingly complex stress state (or stress shadowing effect) during the multiple-stage fracturing simulation. Therefore, the refinement region where the prospective fractures propagate should be extended enough in order not to forcefully limit the accuracy of the solution or the convergence rate. On the other hand, the computational expenses significantly increase using higher number of elements and therefore, mesh refinement should be accomplished carefully.

Acknowledgments

The authors would like to acknowledge Dassault Systemes Simulia Corporation and Chief Oil and Gas Company for providing Abaqus software program and financial support, respectively.

Nomenclature

t = *traction size ($ML^{-1}T^{-2}$), kPa*

t_m^0 = *mixed-mode traction in damage initiation ($ML^{-1}T^{-2}$), kPa*

$\bar{t}$ = *post-damage elastic traction component ($ML^{-1}T^{-2}$), kPa*

K_m = *cohesive layer stiffness ($ML^{-1}T^{-2}$), kPa*

δ_m^0 = *mixed-mode separation in damage initiation (L), m*

δ_m^f = *final mixed-mode separation (L), m*

δ_m^{max} = *maximum mixed-mode separation at partial damage D (L), m*

D = *inviscid cohesive damage variable*

G = *fracture energy release rate (MT^{-2}), kN/m*

G^c = *critical energy release rate (MT^{-2}), kN/m*

$S_{h,min,tot}$ = *total minimum horizontal stress ($ML^{-1}T^{-2}$), kPa*

$S_{H,max,tot}$ = *total maximum horizontal stress ($ML^{-1}T^{-2}$), kPa*

$u^h(x)$ = *displacement at location x (L), m*

$N_I(x)$ = *conventional FEM shape function*

u_I = *nodal degree of freedom (L), m*

$H(x)$ = *Heaviside enrichment function*

a_I = *nodal enrichment degree of freedom for jump discontinuity on fracture walls*

$F_\alpha(x)$ = *crack tip enrichment (asymptotic) function*

b_I^α = *nodal degree of freedom for the crack tip enrichments (L), m*

ϕ = *Porosity*

k = *soil permeability (L^2), mD*

E = *Young's modulus ($ML^{-1}T^{-2}$), GPa*

ν = *Poisson's ratio*

G_{Ic} = *opening-mode energy release rate (MT^{-2}), kN/m*

G_{IIc} = *shearing-mode energy release rate (MT^{-2}), kN/m*

References

1. Platts.com: "US Oil Export Debate: A Platts.com News Feature." Platts, a division of the McGraw-Hill Companies, Inc. ("McGraw-Hill").
2. Cipolla, C.L., Warpinski, N.R., Mayerhofer, M.J. and Lolon, E.P.: "The Relationship between Fracture Complexity, Reservoir Properties, and Fracture Treatment Design." SPE Annual Technical Conference and Exhibition, ATCE2008, Denver, Colorado, September 21-24, 2008.
3. Rickman, R., Mullen, M., Petre, E., Grieser, B. and Kundert, D.: "A practical Use of Shale Petrophysics for Stimulation Design Optimization: All Shale Plays Are Not Clones of the Barnett Shale." SPE Annual Technical Conference and Exhibition, ATCE2008, Denver, Colorado, September 21-24, 2008.
4. Weng, X., Kresse, O., Cohen, C., Wu, R. and Gu, H.: "Modeling of Hydraulic-fracture-network Propagation in a Naturally Fractured Formation." *SPE Journal of Production and Operations* v. 26, No.4, (2011) 368-380.
5. Fjaer, E., Holt, R.M., Horsrud, P., Raaen, A.M. and Risnes, R.: "Petroleum Related Rock Mechanics." *Developments in Petroleum Science* 2nd ed., UK: Elsevier (2008).
6. Mohammadnejad, T. and Khoei, A.R.: "An Extended Finite Element Method for Hydraulic Fracture Propagation in Deformable Porous Media with the Cohesive Crack Model." *Finite Elements in Analysis and Design* v. 73, (2013) 77-95.
7. Hansford, J. and Fisher, Q.: "The Influence of Fracture Closure from Petroleum Production from Naturally Fractured Reservoirs: A Simulation Modeling Approach." AAPG Annual Convention, AAPG2009, Search and Discovery Article No. 40442.
8. Haddad, M. and Sepehrnoori, K.: "Cohesive Fracture Analysis to Model Multiple-stage Fracturing in Quasibrittle Shale Formations." SIMULIA Community Conference, SCC2014, Providence, Rhode Island, May 19-21, 2014. file:///F:/PhD%20Research/papers/2014%20SCC/scc-2014-proceedings.pdf.
9. Haddad, M. and Sepehrnoori, K.: "Simulation of Multiple-stage Fracturing in Quasibrittle Shale Formations Using Pore Pressure Cohesive Zone Model." SPE/AAPG/SEG Unconventional Resources Technology Conference, URTeC2014, Denver, Colorado, August 25-27, 2014. DOI: 10.15530/urtec-2014-1922219.
10. Haddad, M. and Sepehrnoori, K.: "Simulation of Hydraulic Fracturing in Quasi-brittle Shale Formations Using Characterized Cohesive Layer: Stimulation Controlling Factors." *J. Unconventional Oil Gas Resourc* v. 9 (2015) 65-83. DOI: 10.1016/j.juogr.2014.10.001
11. Daneshy, A.: "Hydraulic Fracturing of Horizontal Wells: Issues and Insights." SPE Hydraulic Fracturing Technology Conference and Exhibition, HFTC2011, The Woodlands, Texas, January 24-26, 2011.
12. Adachi, J., Siebrits, E., Peirce, A. and Desroches, J.: "Computer Simulation of Hydraulic Fractures." *International Journal of Rock Mechanics & Mining Sciences* v. 44 (2007) 739-757.
13. Crouch, S.L.: "Solution of Plane Elasticity Problems by the

Displacement Discontinuity Method." *Int. J. Numer. Methods Engrg.* v. 10 (1976) 301-343.
14. Crouch, S.L. and Starfield, A.M.: "Boundary Element Methods in Solid Mechanics." London, England: Allen & Unwin, (1983).
15. Secchi, S. and Schrefler, B.A.: "A Method for 3-D Hydraulic Fracturing Simulation." *Int. J. Fract.* v. 178 (2012) 245-258.
16. Huang, K., Zhang, Z. and Ghassemi, A.: "Modeling Three-dimensional Hydraulic Fracture Propagation Using Virtual Multidimensional Internal Bonds." *Int. J. Numer. Anal. Meth. Geomech.* (2012).
17. Fu, P., Johnson, S.M. and Carrigan, C.R.: "An Explicitly Coupled Hydro-geomechanical Model Simulating Hydraulic Fracturing in Arbitrary Discrete Fracture Networks." *Int. J. Numer. Anal. Meth. Geomech.* (2012).
18. Bazant, Z.P.: "Fracture and Size Effect in Concrete and Other Quasibrittle Materials." Boca Raton: CRC Press LLC, (1998).
19. Gonzalez, M. and Dahi Taleghani, A.: "A Cohesive Model for Modeling Hydraulic Fractures in Naturally Fractured Formations." SPE Hydraulic Fracturing Technology Conference, HFTC2015, Woodlands, Texas, February 3-5, 2015. DOI:10.2118/173384-MS
20. Abaqus Analysis User's Manual, Version 6.14-1, Dassault Systémes Simulia Corp., Providence, RI, 2014.
21. Zielonka, M.G., Searles, K.H., Ning, J. and Buechler, S.R.: "Development and Validation of Fully-coupled Hydraulic Fracturing Simulation Capabilities." SIMULIA Community Conference, SCC2014, Providence, Rhode Island, May 19-21, 2014.
file:///F:/PhD%20Research/papers/2014%20SCC/scc-2014-proceedings.pdf
22. Wong, S., Geilikman, M. and Xu, G.: "The Geomechanical Interaction of Multiple Hydraulic Fractures in Horizontal Wells." Effective and Sustainable Hydraulic Fracturing (ed. R. Jeffrey), (2013). DOI: 10.5772/56385.
23. Belytschko, T. and Black, T.: "Elastic Crack Growth in Finite Elements with Minimal Remeshing." *Int. J. Numer. Meth. Engng* v. 45 (1999) 601-620.
24. Moes, N., Dolbow, J. and Belytschko, T.: "A Finite Element Method for Crack Growth without Remeshing." *International Journal for Numerical Methods in Engineering* v. 46 (1999) 131–150.
25. Babuska, I. and Melenk, J.M.: "The Partition of Unity Method." *Int. J. for Numer. Meth. Engng* v. 40 (1997) 727-758.
26. Song, J., Areias, P.M. and Belytschko, T.: "A Method for Dynamic Crack and Shear Band Propagation with Phantom Nodes." *Int. J. Numer. Meth. Engng* v. 67 (2006) 868-893.
27. Hansbo, A. and Hansbo, P.: "A Finite Element Method for the Simulation of Strong and Weak Discontinuities in Solid Mechanics." *Comput. Methods Appl. Mech. Engng.* v. 193 (2004) 3523-3540.
28. Howard, G.C. and Fast, C.R.: "Optimum Fluid Characteristics for Fracture Extension." Spring meeting of the Mid-Continent District, Division of Production, Tulsa, Oklahoma, April 1957.
29. Haddad, M. and Sepehrnoori, K.: "XFEM-based CZM for the Simulation of 3D Multiple-Stage Hydraulic Fracturing in Quasi-brittle Shale Formations" 5th International Conference on Coupled Thermo-Hydro-Mechanical-Chemical (THMC) Processes in Geosystems: Petroleum and Geothermal Reservoir Geomechanics and Energy Resource Extraction, GeoProc 2015, Salt Lake City, Utah, February 25-27, 2015.
30. Geertsma, J. and de Klerk, F.: "A Rapid Method of Predicting Width and Extent of Hydraulically Induced Fractures." *J. Pet. Technol.* v. 21 (1969) 1571–1581.
31. Abaqus Benchmarks Guide, Version 6.14-1, Dassault Systémes Simulia Corp., Providence, RI, 2014.

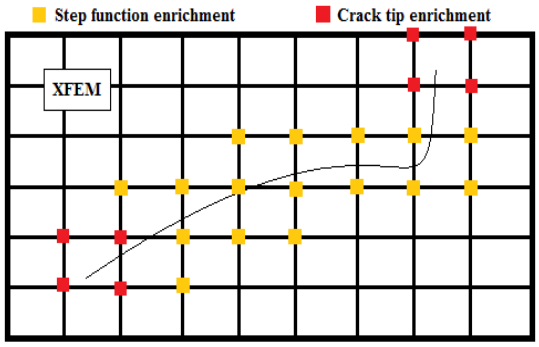

Figure 1: A schematic single fracture enrichment on tips and wall

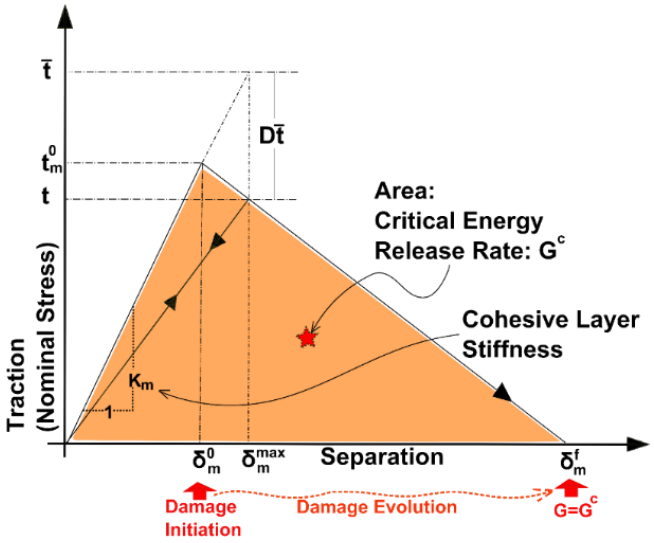

Figure 2: Typical cohesive traction-separation law with linear damage evolution in a Cohesive Zone Model (CZM)[10]. Cohesive behavior is generally constituted of the elastic response followed by progressive damage after fracture initiation.

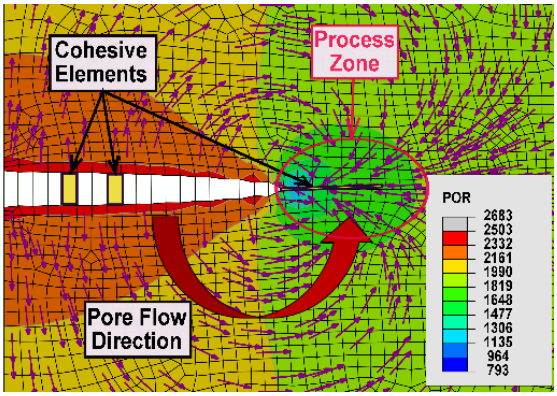

Figure 3: Complex fluid flow pattern around the fracture tip due to the low-pore-pressure region or large matrix deformation (extension) inside the fracture tip process zone[10]. This result was generated using quasi-static, soils consolidation analysis using the planar CZM for fracture propagation in Abaqus.

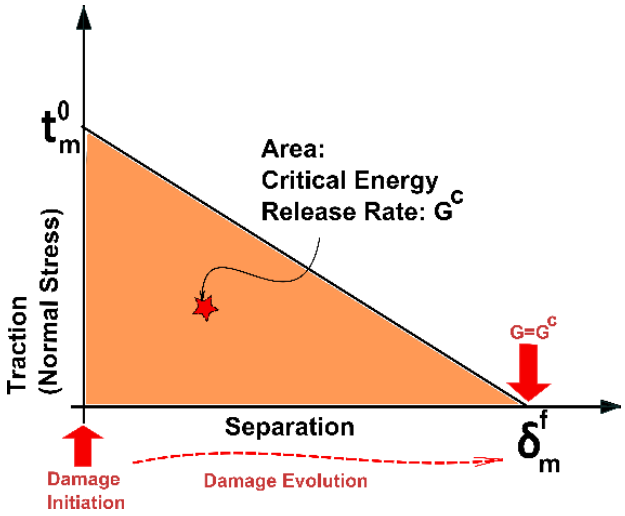

Figure 4: Cohesive traction-separation law in a XFEM-based CZM. The cohesive behavior is only constituted of the progressive damage after fracture initiation.

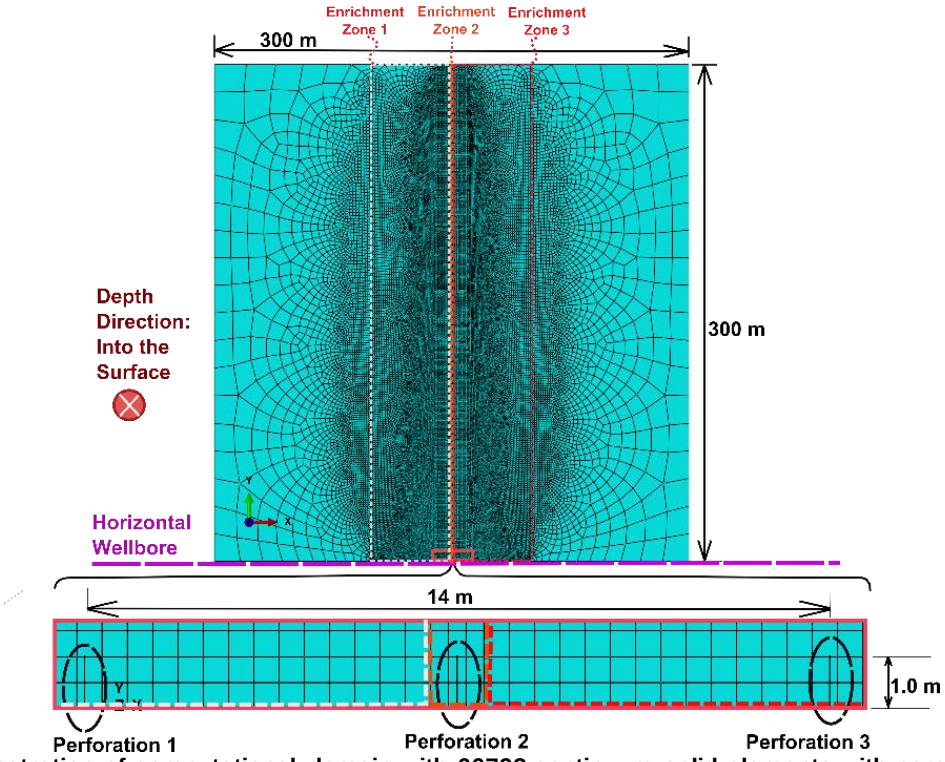

Figure 5: The demonstration of computational domain with 66793 continuum solid elements with pore pressure degree of freedom, C3D8P. The depth direction is into the surface and the geometry thickness is one meter. The initial fractures are spaced by 7 meters up to one meter in length.

Table 1: Parameters for the 3D model with a single layer of C3D8P elements

Properties	Value
Depth [m]	80 (default), 800
Formation Thickness [m]	1.0
$S_{h,min,total}$ [kPa]	1000, 10000
$S_{H,max,total}$ [kPa]	1100, 11000
Initial Reservoir Pore Pressure [kPa]	800, 8000
Initial Porosity, ϕ [] (at zero pore pressure, stress, and zero strain)	0.25
Initial Effective Permeability [mD] (variable with porosity) at initial porosity	2.50
Poisson's Ratio, ν []	0.25
Young's Modulus, E [GPa]	1.294
Critical Energy Release Rate, G_{Ic} and G_{IIc} [kN/m]	28
Damage Initiation Stress, t^o [kPa]	320
Leak-off Coefficient (m^3/kPa.s)	5.879E-10
Stabilization Parameter	0.02 (default), 0.03

Table 2: Operational properties

Parameter	Value
Max. Pump Rate [m^3/sec/cluster]	1.0E-3
Injection Amplitude Curve	Ramp up linearly in the first 200 seconds
Injection Time [sec]	3000
Number of Perforations (clusters per stage)	3
Cluster Spacing [m]	7 (default), 13, 20
Injection Fluid Density [kg/m^3]	1000
Viscosity [cp]	1
Fracturing Fluid Power Law Exponent	0.95

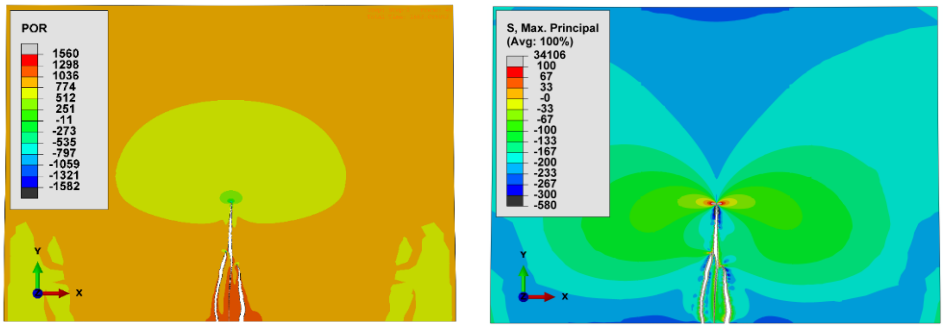

Figure 6: Pore pressure (left) and maximum principal stress (right) contours in kPa after 1683 seconds of simulation for triple-stage simultaneous hydraulic fracturing at 7-meter spacing. Fracture coalescence hindered further time marching. Fracture lengths are 65, 116, and 53 meters left to right. The displacements are magnified 150 times for a better fracture demonstration.

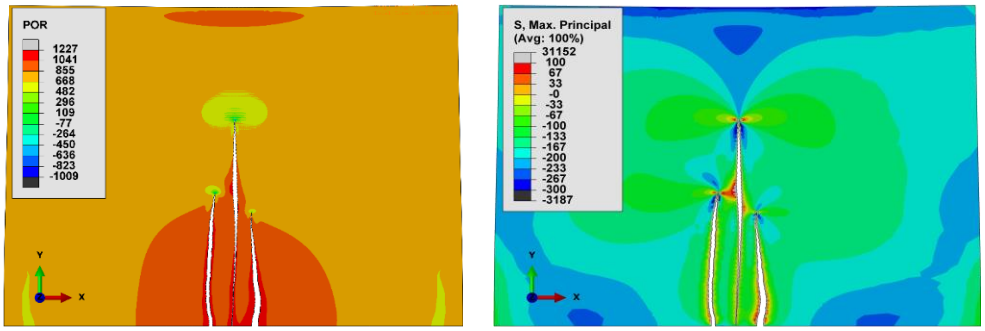

Figure 7: Pore pressure (left) and maximum principal stress (right) contours in kPa after 4000 seconds of simulation for triple-stage simultaneous hydraulic fracturing at 13-meter spacing. Fractures did not coalesce up to the end of simulation. Fracture lengths are 125, 194, and 107 meters left to right. The displacements are magnified 150 times for a better fracture demonstration.

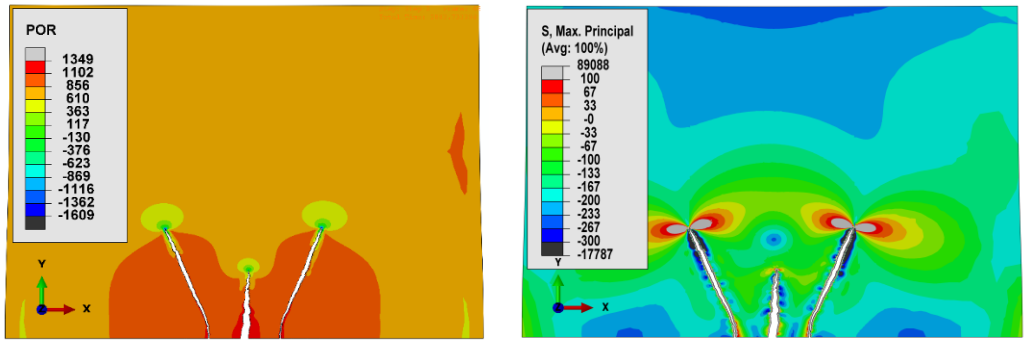

Figure 8: Pore pressure (left) and maximum principal stress (right) contours in kPa after 2883 seconds of simulation for triple-stage simultaneous hydraulic fracturing at 20-meter spacing. Fractures diverged in geometry up to the coarse element region. Fracture lengths are 103, 59, and 103 meters left to right. The displacements are magnified 150 times for a better fracture demonstration.

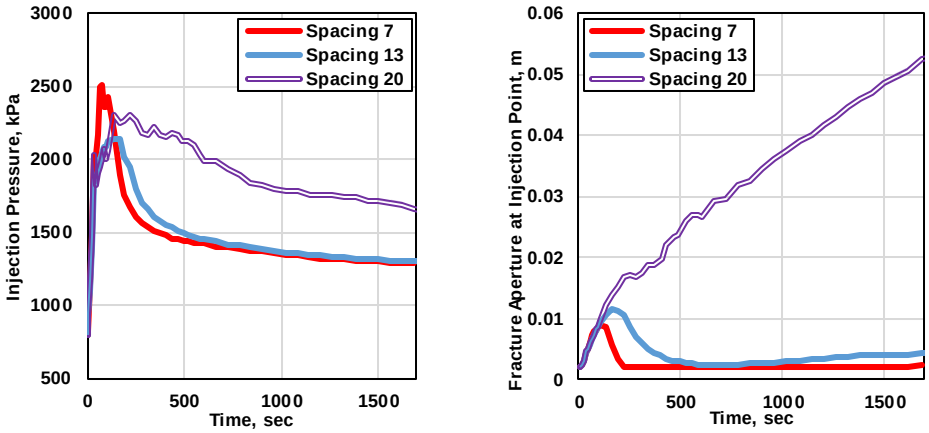

Figure 9: Comparison of the injection pressure (left), and fracture aperture at the injection point (right), both for the middle perforation, at various spacing.

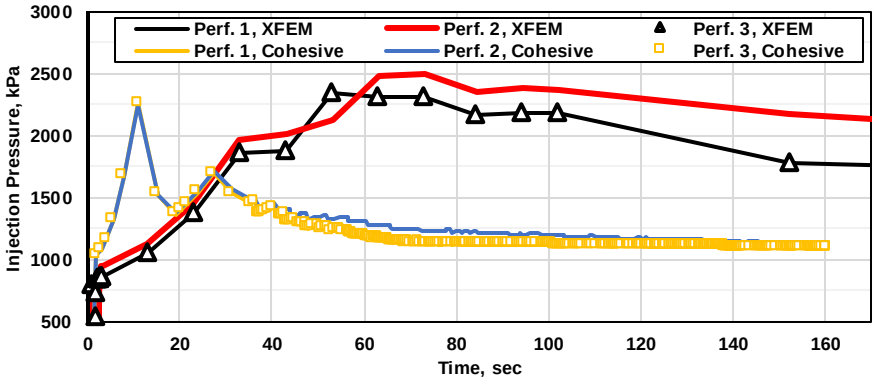

Figure 10: Comparison of the injection pressure at various stages in the planar CZM model (Cohesive in the legends) and XFEM-based CZM model (XFEM in the legends).

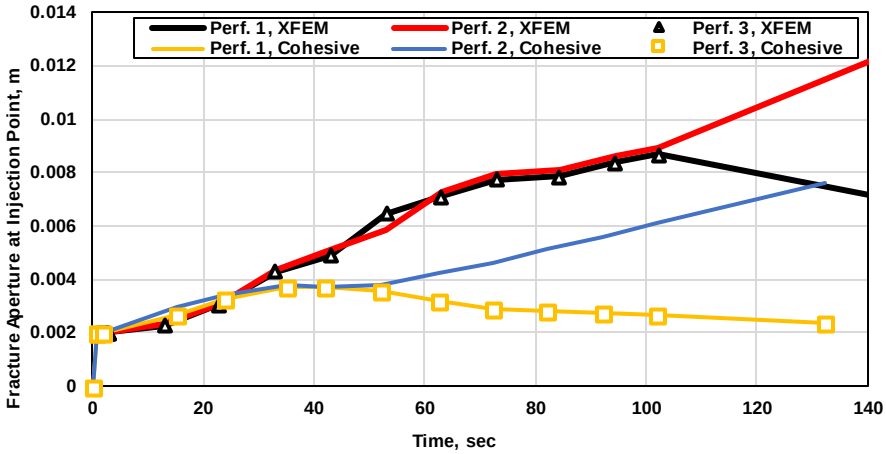

Figure 11: Comparison of the fracture opening (aperture) at the injection point in the planar CZM model (Cohesive in the legends) and XFEM-based CZM model (XFEM in the legends).

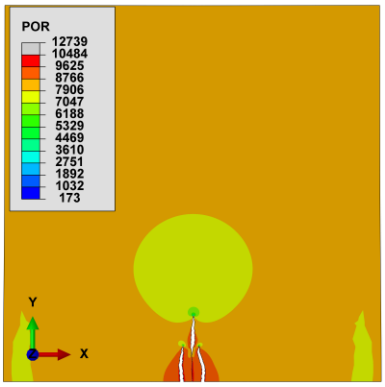

(a) $S_{H,max,tot} = 9900$

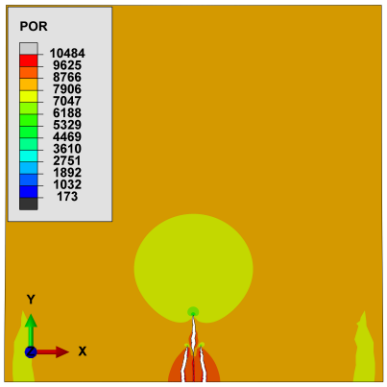

(b) $S_{H,max,tot} = 10000$

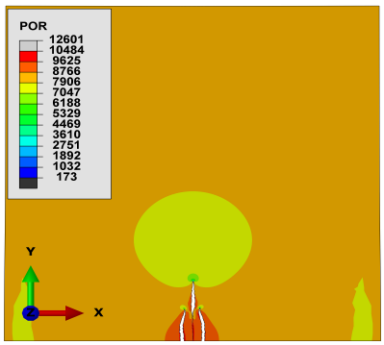

(c) $S_{H,max,tot} = 10100$

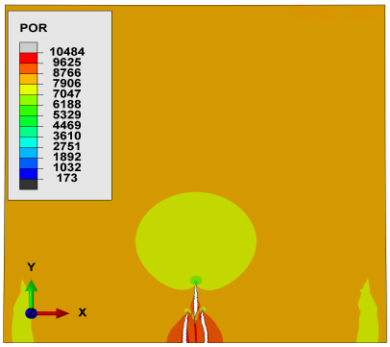

(d) $S_{H,max,tot} = 10200$

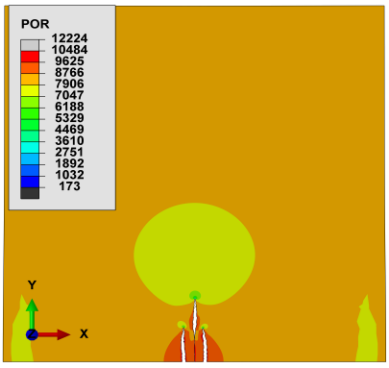

(e) $S_{H,max,tot} = 10500$

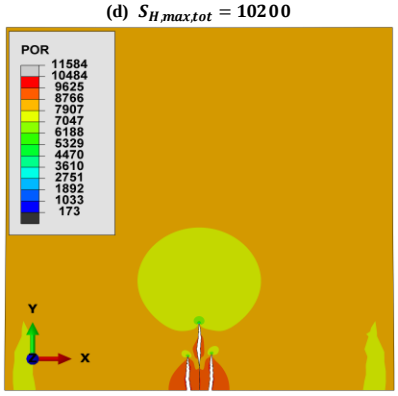

(f) $S_{H,max,tot} = 11000$

Figure 12: Pore pressure contours in kPa at 7-meter spacing for various maximum horizontal stresses, $S_{H,max,tot}$, and constant minimum horizontal stress equal to 10000 kPa, after 1500 seconds of simulation. The initial pore pressure was 8000 kPa. For a better fracture demonstration, the displacements have been amplified 50 times.

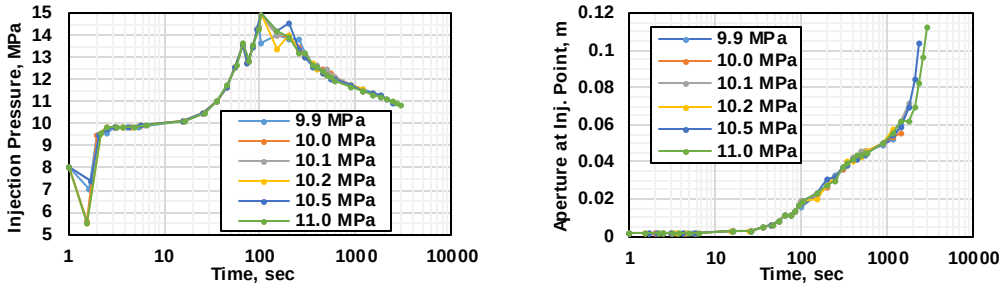

Figure 13: Comparison of the injection pressure (left figure), and fracture aperture or opening at the injection spot (right figure), both for the left perforation, at various maximum horizontal stresses, $S_{H,max}$, and constant minimum horizontal stress, $S_{h,min}$ equal to 10 MPa.

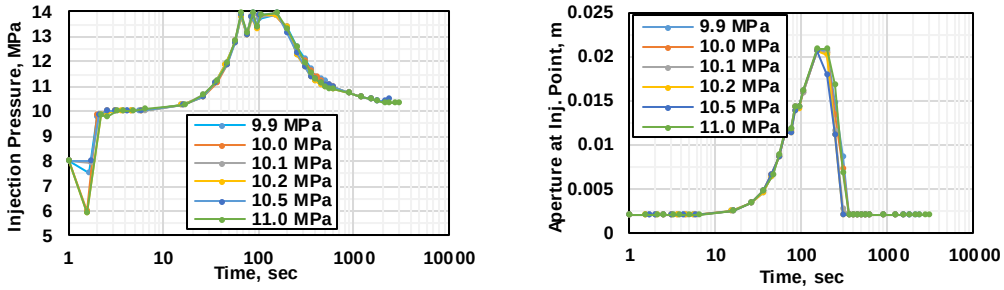

Figure 14: Comparison of the injection pressure (left figure), and fracture aperture or opening at the injection spot (right figure), both for the middle perforation, at various maximum horizontal stresses, $S_{H,max}$, and constant minimum horizontal stress, $S_{h,min}$ equal to 10 MPa.

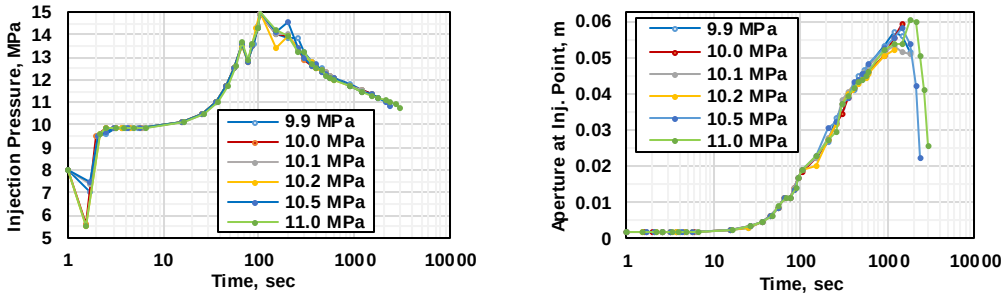

Figure 15: Comparison of the injection pressure (left figure), and fracture aperture or opening at the injection spot (right figure), both for the right perforation, at various maximum horizontal stresses, $S_{H,max}$, and constant minimum horizontal stress, $S_{h,min}$ equal to 10 MPa.